

Kuramoto model for excitation-inhibition-based oscillations

Ernest Montbrió¹ and Diego Pazó²

¹Center for Brain and Cognition. Department of Information and Communication Technologies, Universitat Pompeu Fabra, 08018 Barcelona, Spain

²Instituto de Física de Cantabria (IFCA), CSIC-Universidad de Cantabria, 39005 Santander, Spain
(Dated: November 3, 2021)

The Kuramoto model (KM) is a theoretical paradigm for investigating the emergence of rhythmic activity in large populations of oscillators. A remarkable example of rhythmogenesis is the feedback loop between excitatory (E) and inhibitory (I) cells in large neuronal networks. Yet, although the EI-feedback mechanism plays a central role in the generation of brain oscillations, it remains unexplored whether the KM has enough biological realism to describe it. Here we derive a two-population KM that fully accounts for the onset of EI-based neuronal rhythms and that, as the original KM, is analytically solvable to a large extent. Our results provide a powerful theoretical tool for the analysis of large-scale neuronal oscillations.

The Kuramoto model (KM) is an idealized mathematical model for exploring the birth of collective synchronization in its most simple form. It consists of a population of heterogeneous, all-to-all coupled oscillators, and is a unique example of exactly solvable system of nonlinear differential equations [1–5]. Yet, the KM was originally not intended as a specific description of any particular system, and finds limited applications in the modeling and analysis of natural oscillatory phenomena, see e.g. [6–8].

An important example of collective synchronization are large scale neuronal oscillations [3, 9]. Despite continued work using the KM to investigate neuronal rhythms (see e.g. [10–16]), it remains unknown whether the KM actually accounts for the neuronal mechanisms resulting in such oscillations. In this Letter we derive a simple, two-population KM, that describes one of the basic mechanisms of generation of neuronal oscillations: The feedback loop between fast excitation (E) and slow inhibition (I) in large neuronal networks [17–20].

EI-feedback loop and EI-based oscillations: The canonical neuronal network to model the EI-feedback loop consists of two interacting populations of excitatory and inhibitory neurons [21–24]. Here, we consider two populations of N pulse-coupled “Winfree oscillators” [2, 25–29] with phase variables $\{\theta_i^\sigma\}_{i=1,\dots,N}$ (populations are identified by $\sigma \in \{E, I\}$), which evolve according to

$$\dot{\theta}_i^\sigma = \omega_i^\sigma + \xi_i^\sigma + Q(\theta_i^\sigma) (K_{\sigma E} h_E - K_{\sigma I} h_I). \quad (1)$$

The natural frequencies ω_i^σ are drawn from Lorentzian distributions of half-width γ , centered at $\bar{\omega}_\sigma$

$$g_\sigma(\omega) = (\gamma/\pi) [(\omega - \bar{\omega}_\sigma)^2 + \gamma^2]^{-1}, \quad (2)$$

and ξ_i^σ are independent, zero-mean delta-correlated noise processes of strength D : $\langle \xi_i^\sigma(t) \xi_j^{\sigma'}(t') \rangle = 2D\delta(t-t')\delta_{i,j}\delta_{\sigma,\sigma'}$. In Eq. (1), $Q(\theta)$ is the so-called phase response curve (PRC) that determines the response of the oscillators to perturbations. Here we adopt the (infinitesimal) PRC of the theta-neuron model, $Q(\theta) = 1 - \cos \theta$, which is nonnegative and thus results in phase advances/delays in response to excitatory/inhibitory inputs [30–32]. Neuronal oscillators with non-negative PRC are called Type 1, and include a broad class of

neuronal models, see e.g. [31–33]. The oscillators interact all-to-all via the mean fields

$$h_\sigma = \frac{1}{N} \sum_{j=1}^N P(\theta_j^\sigma), \quad (3)$$

which are population-averaged sums of all the pulses P produced in each population. We use the family of unimodal even-symmetric functions $P(\theta) = (1 - r)(1 + \cos \theta)(1 - 2r \cos \theta + r^2)^{-1}$, with $\int_{-\pi}^{\pi} P(\theta) d\theta = 2\pi$ and a free parameter $r \in (-1, 1)$, such that $\lim_{r \rightarrow 1} P(\theta) = 2\pi\delta(\theta)$ [28]. Expressed in words, the j -th oscillator in the E population exerts a positive, pulse-like influence $P(\theta_j^E)$ of strength $K_{EE}/N \geq 0$ to each oscillator of the E population, and of strength $K_{IE}/N \geq 0$ to each oscillator of the I population (similarly for the j -th oscillator of the I population, with an explicit “−” sign in Eq. (1) corresponding to inhibition).

Figure 1(a,b) shows EI-based oscillations of the mean-field quantities h_σ in simulations of (a) heterogeneous and (b) noisy

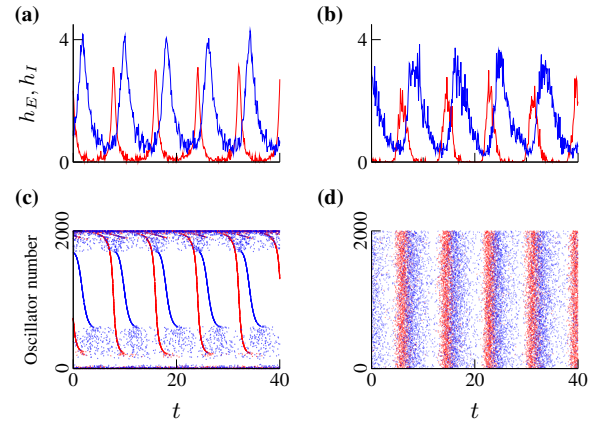


FIG. 1. EI-based oscillations in a population of $N = 2000$ excitatory (E) and $N = 2000$ inhibitory (I) Winfree oscillators, Eq. (1); with $\bar{\omega}_E = 1.5$, $\bar{\omega}_I = 0.5$, $K_{EI} = K_{IE} = 0.5$, $K_{EE} = K_{II} = 0$, and $r = 0.99$. (a,b) Time series of the E (red) and I (blue) activity-based mean fields h_σ . (c,d) Raster plots: A point is plotted when an oscillator’s phase reaches a multiple of 2π , which is the peak location of $P(\theta)$. In (a,c) frequencies are Lorentzian distributed, with $\gamma = 0.1$, and $D = 0$. In (b,d) the noise strength is $D = 0.1$, and $\gamma = 0$.

EI-Winfree networks, Eqs (1). The raster plots Figs.1(c,d) show that an EI-oscillation cycle begins with the synchronous ‘firing’ of a large cluster of phase-locked E-oscillators, followed by another synchronous ‘firing’ of the I-oscillators. Note that, to emphasize that oscillations emerge exclusively due to the interplay between fast excitatory and slow inhibitory dynamics, in Fig. (1) we set the self-coupling terms to zero, $K_{EE} = K_{II} = 0$, and consider $\Delta\omega \equiv \bar{\omega}_E - \bar{\omega}_I > 0$. In the following we derive a two-population KM that captures the main features of the oscillations shown in Fig. (1), and that is exactly solvable to a large extent.

Excitation-Inhibition Kuramoto model (EI-KM): Invoking the averaging approximation, valid for weak coupling and nearly identical oscillators [1, 3], the EI-Winfree model in Eq. (1) reduces to the EI-KM [34]

$$\begin{aligned} \dot{\theta}_i^\sigma &= \tilde{\omega}_i^\sigma + \xi_i^\sigma \\ &- \frac{1+r}{2N} \sum_{j=1}^N [K_{\sigma E} \cos(\theta_i^\sigma - \theta_j^E) - K_{\sigma I} \cos(\theta_i^\sigma - \theta_j^I)], \end{aligned} \quad (4)$$

where $\tilde{\omega}_i^\sigma \equiv \omega_i^\sigma + K_{\sigma E} - K_{\sigma I}$. There are two major differences between the EI-KM and the classical single and two-population KM broadly investigated in the literature, see e.g. [1, 35–40]. First, in the EI-KM the excitatory and inhibitory coupling constants differentially shift the natural frequencies $\tilde{\omega}_i^E$ and $\tilde{\omega}_i^I$, and this largely affects the regions of parameters where EI-oscillations occur. Second, although the cosine coupling does not promote synchrony in the KM [41], the positive (E) and negative (I) cross-coupling terms in Eqs. (4) crucially conspire to synchronize the oscillators [42]. Therefore, in the EI-KM synchrony sets in exclusively due to the cooperative action of both the E and the I populations, in consonance with the EI-feedback loop mechanism. Indeed, Fig. 2 shows numerical simulations of the EI-KM in Eqs. (4) using the same parameters as in Fig. 1(a,c) —except r , which in the EI-KM is set to $r = 1$, see below. Fig. 2(a) displays the amplitude of the complex Kuramoto order parameters $Z_\sigma \equiv R_\sigma e^{i\Psi_\sigma} = N^{-1} \sum_{j=1}^N e^{i\theta_j^\sigma}$. At $t = 0$, the amplitudes R_E and R_I are near zero since the initial values of all the phases are randomly distributed in the interval $[0, 2\pi)$. Then, after a brief transient, the Kuramoto order parameters converge (up to finite-size fluctuations) to uniformly rotating solutions $Z_\sigma(t) = R_* e^{i\Psi_\sigma(t)}$, with $0 < R_* < 1$ and $\dot{\Psi}_\sigma = \Omega$, signaling the onset of collective synchronization. Note that the raster plot in Fig. 2(b) shows that the cluster of E oscillators precedes the cluster of I oscillators, consistent with Fig. 1(c).

Finally, in the EI-KM the width of the pulses (controlled by r) influences the intensity of the cosine coupling functions. To lighten the notation, hereafter we set $r = 1$ in Eqs. (4), corresponding to the limit of infinitely narrow (Dirac delta) pulses —this is close to the value used in Fig. (1). The generalization of our results to general r is trivial.

Analysis of the EI-KM: Eqs. (4) can be efficiently analyzed in the thermodynamic limit, $N \rightarrow \infty$. To do so, the discrete sets of phases and frequencies turn into continuous vari-

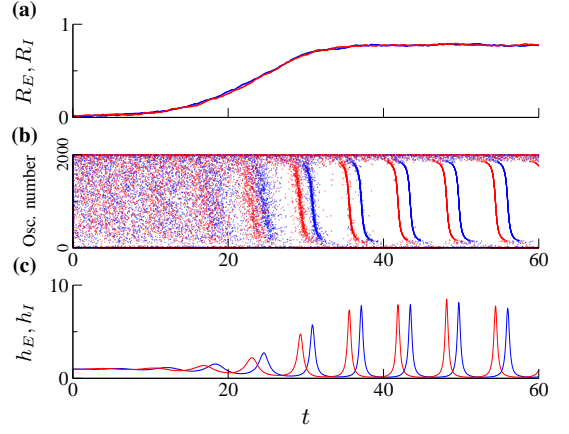


FIG. 2. EI-based oscillations in the EI-KM Eq. (4) with quenched heterogeneity and $N = 2000$. (a) Amplitude of the Kuramoto order parameters, R_E (red) and R_I (blue); (b) Raster plots; (c) Mean fields obtained applying Eq. (14) to Z_σ ; Parameters are as in Fig. 1(a,c), except that here $r = 1$, instead of $r = 0.99$.

ables $\{\theta_i^\sigma, \omega_i^\sigma\} \rightarrow \{\theta_\sigma, \omega_\sigma\}$, and the corresponding probability density functions $f^\sigma(\theta_\sigma | \omega_\sigma, t)$ satisfy coupled the Fokker-Planck equations

$$\partial_t f^\sigma = -\partial_{\theta_\sigma} (f^\sigma \dot{\theta}_\sigma) + D \partial_{\omega_\sigma}^2 f^\sigma, \quad (5)$$

for which the fully incoherent state $f^E = f^I = (2\pi)^{-1}$ is always a trivial solution [35, 43]. It is convenient to introduce the Fourier expansion of f^σ :

$$f^\sigma(\theta | \omega, t) = \frac{1}{2\pi} \sum_{l=-\infty}^{\infty} f_l^\sigma(\omega, t) e^{il\theta}, \quad (6)$$

where $f_0^\sigma = 1$ and $(f_{-l}^\sigma)^* = f_l^\sigma$ (the asterisk denotes complex conjugate). Thus, the Kuramoto order parameters are

$$Z_\sigma = \left[\int_{-\infty}^{\infty} f_1^\sigma(\omega, t) g_\sigma(\omega) d\omega \right]^*. \quad (7)$$

Substituting Eq. (6) into Eq. (5), yields two infinite sets of integro-differential equations for the Fourier modes

$$\begin{aligned} \dot{f}_l^\sigma &= -(il\tilde{\omega}_\sigma + l^2 D) f_l^\sigma + \frac{il}{2} f_{l-1}^\sigma (K_{\sigma E} Z_E^* - K_{\sigma I} Z_I^*) \\ &+ \frac{il}{2} f_{l+1}^\sigma (K_{\sigma E} Z_E - K_{\sigma I} Z_I), \end{aligned} \quad (8)$$

where $\tilde{\omega}_\sigma \equiv \omega_\sigma + K_{\sigma E} - K_{\sigma I}$. The stability of the incoherent state can be analyzed by linearizing Eq. (8) [44]. To simplify the analysis, we study the case in which cross- and self-couplings are symmetric,

$$K_{EI} = K_{IE} \equiv K, \quad K_{II} = K_{EE} \equiv \epsilon K, \quad (9)$$

and use the new parameter $\epsilon \geq 0$ as a measure of the ratio of self- to cross-coupling. Then we find that the eigenvalues determining the stability of incoherence are

$$\lambda_\pm = -\gamma - D \pm \frac{1}{2} \sqrt{K^2 - [\Delta\omega + (\epsilon - 2)K]^2} - i\Omega, \quad (10)$$

where $\Omega = (\bar{\omega}_E + \bar{\omega}_I)/2$ is the center of the frequency distribution combining E and I populations. Note that parameters γ and D play identical roles in Eq. (10), as it occurs in the KM [43]. Imposing $\text{Re}(\lambda_+) = 0$ in Eq. (10), we find the boundary of incoherence

$$\left(\frac{\Delta\omega}{\gamma + D}\right)_c^\pm = (2 - \epsilon)\frac{K}{\gamma + D} \pm \sqrt{\left(\frac{K}{\gamma + D}\right)^2 - 4}, \quad (11)$$

which is the family of hyperbolas depicted by solid and dashed black lines in Figs. 3(a-d), for increasing values of ϵ . A necessary condition for the boundary Eq. (11) to exist is

$$\frac{K}{\gamma + D} \geq 2. \quad (12)$$

Hence, given a certain level of heterogeneity and/or noise, synchronization sets in at large enough values of the coupling strength. This is remarkably similar to the KM [1, 43], although here K represents cross-, and not self-coupling. Moreover, Eq. (12) is not a sufficient condition for synchronization in the EI-KM. If Eq. (12) is satisfied, then Eq. (11) shows that synchronization is only achieved for a particular range of values of the frequency mismatch $\Delta\omega$. The coupling ratio ϵ does not affect Eq. (12), but it critically controls the range of $\Delta\omega$ for stable incoherence: Note that when $\epsilon \leq 1$, the boundary Eq. (11) is located at positive values of $\Delta\omega$, and thus incoherence is always stable when I oscillators are intrinsically faster than E oscillators ($\Delta\omega < 0$), see Fig. (3). Increasing the parameter ϵ shifts the boundary, with asymptotes at $K = \Delta\omega/(3 - \epsilon)$ and $K = \Delta\omega/(1 - \epsilon)$, towards negative values of $\Delta\omega$. Thus, increasing the coupling ratio through ϵ provides a key ingredient for synchronizing EI networks when $\bar{\omega}_I > \bar{\omega}_E$, as I-to-I coupling slows down I oscillators while E-to-E coupling speeds up E oscillators.

The synchronization region turns out to be larger than the hyperbolic boundary defined by Eq. (11), particularly for large ϵ values (see Fig. 3 for the noise-free case). The reason is that the bifurcation at Eq. (11) is often sub-critical. To investigate this further, next we consider the purely heterogeneous ($D = 0$) and the purely noisy ($\gamma = 0$) cases separately, and show that the global picture is remarkably similar in both instances.

The noise-free problem is particularly simple since it can be assumed that the densities in Eq. (6) satisfy the so-called Ott-Antonsen (OA) ansatz [45, 46]

$$f_{l>1}^\sigma(\omega, t) = [f_1^\sigma(\omega, t)]^l. \quad (13)$$

A first useful outcome of the OA ansatz is that it allows to infer the mean field h_σ , Eq. (3), from the Kuramoto order parameter Z_σ , Eq. (7). Specifically, in the thermodynamic limit $h_\sigma(t) = \int_{-\infty}^{\infty} \int_0^{2\pi} P(\theta) f^\sigma(\theta|\omega, t) g_\sigma(\omega) d\omega d\theta$. Then, considering $P(\theta)$ as defined above, and the heterogeneity in Eq. (2), one finds $h_\sigma = \text{Re}[(1 + Z_\sigma)/(1 - r Z_\sigma)]$, see [47]. In the limit $r \rightarrow 1$, this relation reduces to

$$h_\sigma = (1 - R_\sigma^2)(1 + R_\sigma^2 - 2R_\sigma \cos \Psi_\sigma)^{-1}. \quad (14)$$

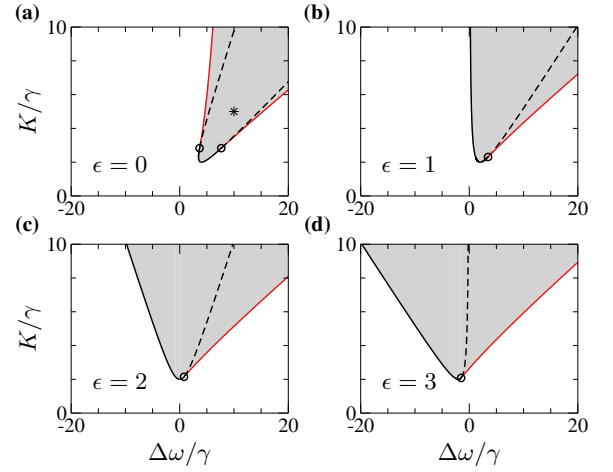


FIG. 3. Phase diagrams of the EI-KM Eq. (4) with $D = 0$ and coupling constants given by Eq. (9), for various values of ϵ . Regions of stable synchronization are highlighted in gray. Synchronization and incoherence are both stable in regions limited by black-dashed and red lines. The asterisk in (a) marks the parameter values used in Fig. 2. Black lines correspond to Eq. (11). Solid and dashed lines are separated by codimension-2 points—obtained from Eq. (19)—, and indicate super/sub-critical bifurcations, respectively. Red curves indicate saddle-node bifurcations.

Figure 2(c) displays the mean fields $h_\sigma(t)$ obtained applying Eq. (14) to the Kuramoto order parameters $Z_\sigma(t)$ of the EI-KM. It can be seen that uniformly rotating solutions of the Kuramoto order parameters correspond to pulsatile oscillations of the activity-based mean fields $h_\sigma(t)$ [48]. Though the agreement between Figs. 1(a) and 2(c) is only qualitative, it gradually improves as parameters γ and $\Delta\omega$ are decreased and the averaging approximation becomes more accurate [49].

A major simplification occurs assuming that f^σ evolve in the so-called OA manifold, Eq. (13), as the system of Eqs. (8) becomes independent of the index l . Then, solving the integrals in Eq. (7) by virtue of the residue theorem, we find a system of two complex-valued ordinary differential equations for the $Z_\sigma(t) = f_1^\sigma(\omega = \bar{\omega}_\sigma - i\gamma, t)^*$

$$\dot{Z}_\sigma = i \left[\hat{\omega}_\sigma Z_\sigma - \frac{K_{\sigma E}}{2} (Z_\sigma^2 Z_E^* + Z_E) + \frac{K_{\sigma I}}{2} (Z_\sigma^2 Z_I^* + Z_I) \right], \quad (15)$$

with $\hat{\omega}_\sigma \equiv \bar{\omega}_\sigma + K_{\sigma E} - K_{\sigma I} + i\gamma$. Restricting our analysis to the case defined by Eqs. (9), Eqs. (15) reduce to a three dimensional system for the amplitudes R_σ and the phase difference $\Phi \equiv \Psi_E - \Psi_I$. The analysis becomes further facilitated restricting to the symmetric subspace

$$R_E = R_I \equiv R, \quad (16)$$

in consistency with our numerical observations, the transverse stability of the fixed points [50], and related work [51]. Hence we analyze the planar system

$$\dot{R} = R \left[-\gamma + \frac{K}{2} (1 - R^2) \sin \Phi \right], \quad (17a)$$

$$\dot{\Phi} = \Delta\omega + K \left[(1 + R^2) \cos \Phi - 2 + \epsilon(1 - R^2) \right]. \quad (17b)$$

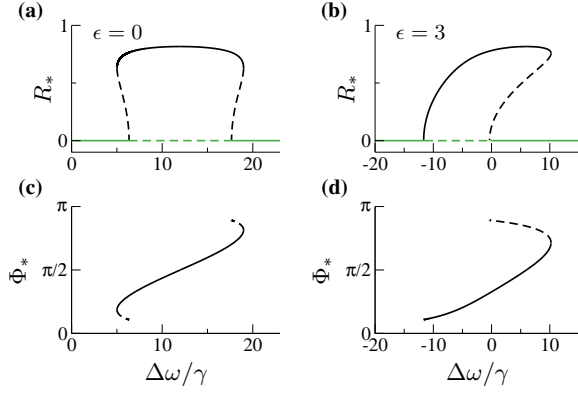


FIG. 4. Bifurcation diagrams of synchronized (black) and incoherent (green) states of Eqs. (17) for $K/\gamma = 6$, obtained using Eq. (18). (a,b) Amplitude R_* and (c,d) Phase difference Φ_* between the Kuramoto order parameters for (a,c) $\epsilon = 0$ and (b,d) $\epsilon = 3$.

Besides the fixed point at $R_* = 0$, corresponding to incoherence, the nontrivial fixed points of Eqs. (17) satisfy [52]

$$\frac{\Delta\omega}{\gamma} = [2 + \epsilon(R_*^2 - 1)] \frac{K}{\gamma} \pm (R_*^2 + 1) \sqrt{\frac{K^2}{\gamma^2} - \frac{4}{(1 - R_*^2)^2}}. \quad (18)$$

Figure 4(a) displays R_* obtained from Eq. (18) for $\epsilon = 0$. In this case the transitions to synchronization are hysteretic and the stable synchronized solution (solid black line) exists only in an interval of values of $\Delta\omega > 0$. As the self-coupling terms are increased, Fig. 4(b) shows that the region of stable synchronization becomes broader, and invades negative values of $\Delta\omega$, see also Figs. 3(a)-(d). Note that the phase difference Φ_* between Z_E and Z_I increases monotonically with $\Delta\omega$, see Figs. 4(c,d), but lies within the interval $(0, \pi)$, and thus excitation always precedes inhibition, see also Eq. (17a).

Differentiating Eq. (18) with respect to R_*^2 and equating the result to zero, allows to analytically obtain the red boundaries in Fig. 3 in parametric form (not shown), corresponding to saddle-node bifurcations. As $R_* \rightarrow 0$, these bifurcations meet the boundaries Eq. (11) at codimension-2 points where the instabilities change from sub- to super-critical. The exact value of the K coordinate is

$$(K/\gamma)_{c2}^{\pm} = \sqrt{(8 - 2\epsilon^2 \mp 2\epsilon\sqrt{8 + \epsilon^2}) / (1 - \epsilon^2)}. \quad (19)$$

Substituting these values into Eq. (11) with $D = 0$, we find the location of the codimension-two points represented in Fig. 3.

Finally, we have numerically verified that very similar bistability regions appear in the phase diagrams for the noisy EI-Kuramoto model Eq. (4) with identical oscillators ($D > 0$, $\gamma = 0$). In addition, following [53], we found that the codimension-2 points of the noisy EI-KM are located at [54]

$$(K/D)_{c2}^{\pm} = \sqrt{(12 - 2\epsilon^2 \mp 2\epsilon\sqrt{24 + \epsilon^2}) / (1 - \epsilon^2)}, \quad (20)$$

which is strikingly similar to Eq. (19), but here the points lie at slightly larger K values.

Conclusions: Using the averaging approximation we derived a two-population Kuramoto model—that we call EI-KM—from an EI-network of pulse-coupled, Type 1 oscillators. The resulting EI-KM displays a transition to synchronization that has the main features of the EI-based (also known as PING, pyramidal-interneuron gamma) rhythms [17–24]: (i) Oscillations set in exclusively due to the cooperative action of both E and I populations. (ii) Oscillations emerge if excitatory dynamics is faster than inhibition, irrespective of ϵ . (iii) Otherwise, when inhibition is faster than excitation, strong enough self-coupling ($\epsilon > 1$) is necessary for synchrony to occur. (iv) Excitation always precedes inhibition ($0 < \Phi_* < \pi$). (v) The transition between incoherence and synchronization is often hysteretic, see e.g. [23]. While these results have been rigorously demonstrated in the EI-KM with Lorentzian heterogeneities (by means of the OA ansatz), perturbative and numerical analysis of the EI-KM with noise reveal the same global picture.

We acknowledge support by MINECO (Spain) under Projects No. FIS2016-74957-P, No. PSI2016-75688-P and No. PCIN-2015-127. We also acknowledge support by the European Union’s Horizon 2020 research and innovation programme under the Marie Skłodowska-Curie grant agreement No. 642563.

-
- [1] Y. Kuramoto, *Chemical Oscillations, Waves, and Turbulence* (Springer-Verlag, Berlin, 1984).
 - [2] S. H. Strogatz, *Physica D* **143**, 1 (2000).
 - [3] A. S. Pikovsky, M. G. Rosenblum, and J. Kurths, *Synchronization, a Universal Concept in Nonlinear Sciences* (Cambridge University Press, Cambridge, 2001).
 - [4] J. A. Acebrón, L. L. Bonilla, C. J. Pérez-Vicente, F. Ritort, and R. Spigler, *Rev. Mod. Phys.* **77**, 137 (2005).
 - [5] A. Pikovsky and M. Rosenblum, *Chaos* **25**, 097616 (2015).
 - [6] K. Wiesenfeld, P. Colet, and S. H. Strogatz, *Phys. Rev. Lett.* **76**, 404 (1996).
 - [7] S. H. Strogatz, D. M. Abrams, A. McRobie, B. Eckhardt, and E. Ott, *Nature* **438**, 43 (2005).
 - [8] I. Z. Kiss, Y. Zhai, and J. L. Hudson, *Science* **296**, 1676 (2002).
 - [9] G. Buzsáki, *Rhythms of the Brain* (Oxford University Press, 2006).
 - [10] M. Breakspear, S. Heitmann, and A. Daffertshofer, *Frontiers in human neuroscience* **4** (2010).
 - [11] J. Cabral, E. Hugues, O. Sporns, and G. Deco, *NeuroImage* **57**, 130 (2011).
 - [12] R. Ton, G. Deco, and A. Daffertshofer, *PLOS Comput Biol* **10**, e1003736 (2014).
 - [13] P. Villegas, P. Moretti, and M. A. Muñoz, *Sci. Rep.* **4** (2014).
 - [14] A. Ponce-Alvarez, G. Deco, P. Hagmann, G. L. Romani, D. Mantini, and M. Corbetta, *PLoS Comput. Biol.* **11**, e1004100 (2015).
 - [15] P. Sanz-Leon, S. A. Knock, A. Spiegler, and V. K. Jirsa, *NeuroImage* **111**, 385 (2015).
 - [16] S. Petkoski, A. Spiegler, T. Proix, P. Aram, J.-J. Temprado, and V. K. Jirsa, *Phys. Rev. E* **94**, 012209 (2016).
 - [17] M. Whittington, R. Traub, N. Kopell, B. Ermentrout, and E. Buhl, *Int. Journal of Psychophysiol.* **38**, 315 (2000).

- [18] P. Tiesinga and T. J. Sejnowski, *Neuron* **63**, 727 (2009).
- [19] X.-J. Wang, *Physiological reviews* **90**, 1195 (2010).
- [20] G. Buzsáki and X.-J. Wang, *Annual Review of Neuroscience* **35**, 203 (2012).
- [21] H. R. Wilson and J. D. Cowan, *Biophys. J.* **12**, 1 (1972).
- [22] N. Brunel and X.-J. Wang, *Journal of neurophysiology* **90**, 415 (2003).
- [23] D. Hansel and G. Mato, *Neural Computation* **15**, 1 (2003).
- [24] C. Boergers and N. Kopell, *Neural Computation* **15**, 509 (2003).
- [25] A. T. Winfree, *J. Theor. Biol.* **16**, 15 (1967).
- [26] J. T. Ariaratnam and S. H. Strogatz, *Phys. Rev. Lett.* **86**, 4278 (2001).
- [27] D. Pazó and E. Montbrió, *Phys. Rev. X* **4**, 011009 (2014).
- [28] R. Gallego, E. Montbrió, and D. Pazó, *Phys. Rev. E* **96**, 042208 (2017).
- [29] C. R. Laing, *Physics* **7**, 10 (2014).
- [30] B. Ermentrout and N. Kopell, *SIAM J. Appl. Math.* **46**, 233 (1986).
- [31] B. Ermentrout, *Neural Comp.* **8**, 979 (1996).
- [32] E. M. Izhikevich, *Dynamical Systems in Neuroscience* (The MIT Press, Cambridge, Massachusetts, 2007).
- [33] E. Brown, J. Moehlis, and P. Holmes, *Neural Computation* **16**, 673 (2004).
- [34] Phase variables in Eqs. (4) correspond to slow-phase approximations of the phases in Eqs. (1). See Supplemental Material, Section I.A.
- [35] H. Okuda and Y. Kuramoto, *Prog. Theor. Phys.* **86**, 1159 (1991).
- [36] E. Montbrió, J. Kurths, and B. Blasius, *Phys. Rev. E* **70**, 056125 (2004).
- [37] E. Barreto, B. Hunt, E. Ott, and P. So, *Phys. Rev. E* **77**, 036107 (2008).
- [38] D. M. Abrams, R. Mirollo, S. H. Strogatz, and D. A. Wiley, *Phys. Rev. Lett.* **101**, 084103 (2008).
- [39] Y. Kawamura, H. Nakao, K. Arai, H. Kori, and Y. Kuramoto, *Chaos* **20**, 043110 (2010).
- [40] B. Pietras, N. Deschle, and A. Daffertshofer, *Phys. Rev. E* **94**, 052211 (2016).
- [41] H. Sakaguchi and Y. Kuramoto, *Prog. Theor. Phys.* **76**, 576 (1986).
- [42] Using $\phi_i^E \equiv \theta_i^E - \pi/2$, Eqs. (4) transform into a two-population model with phases $\{\phi_i^E\}$, $\{\theta_i^I\}$, where self-interaction functions remain the same, while cross-interaction functions become sine functions with the precise signs to favor synchrony. Hence, for the case $K_{EE} = K_{II} = 0$ considered in Fig. 2, the system reduces to a bipartite network of Kuramoto oscillators.
- [43] S. H. Strogatz and R. E. Mirollo, *J. Stat. Phys.* **63**, 613 (1991).
- [44] See the Supplemental Material, Section II.
- [45] E. Ott and T. M. Antonsen, *Chaos* **18**, 037113 (2008).
- [46] E. Ott and T. M. Antonsen, *Chaos* **19**, 023117 (2009).
- [47] See Supplemental Material, Section III.B and [28].
- [48] In Section III.A of the Supplemental Material we show that, in the EI-KM, the mean field h_σ is linearly related with the *mean firing rate* of the population of oscillators that, compared to h_σ , is a more natural measure of neuronal activity in neuroscience.
- [49] See Supplemental Material, Section I.B.
- [50] See Supplemental Material, Section III.A.
- [51] E. A. Martens, E. Barreto, S. H. Strogatz, E. Ott, P. So, and T. M. Antonsen, *Phys. Rev. E* **79**, 026204 (2009).
- [52] In contrast with the KM with bimodal frequency distribution [1, 40, 51, 55–58], our numerical simulations did not reveal states with time-varying R_σ . The same occurs in other variants of the KM, see e.g. [59].
- [53] A. Pikovsky and S. Ruffo, *Phys. Rev. E* **59**, 1633 (1999).
- [54] See Supplemental Material, Section IV.
- [55] J. D. Crawford, *J. Stat. Phys.* **74**, 1047 (1994).
- [56] L. L. Bonilla, J. C. Neu, and R. Spigler, *J. Stat. Phys.* **67**, 313 (1992).
- [57] E. Montbrió, D. Pazó, and J. Schmidt, *Phys. Rev. E* **74**, 056201 (2006).
- [58] D. Pazó and E. Montbrió, *Phys. Rev. E* **80**, 046215 (2009).
- [59] H. Hong and S. H. Strogatz, *Phys. Rev. E* **85**, 056210 (2012).